POLITECNICO DI TORINO

MASTER's Degree in Energy and Nuclear Engineering

Politecnico di Torino

LIÈGE université

Master's Degree Thesis

Impact of Tariff Schemes on Distribution Network Expansion Planning: a Comparative Framework

Supervisor

Prof. Gianfranco CHICCO

Co-supervisor

Prof. Bertrand CORNÉLUSSE

Candidate

Francesco MOGLIA

A.Y. 2024/2025

November 2025

Abstract

Achieving Europe's decarbonization objectives requires a deep electrification of end-use sectors. This transition, while indispensable, imposes unprecedented stress on distribution networks, which must accommodate higher peak loads, bidirectional power flows from distributed generation, and increased variability from weather-dependent sources. Addressing these challenges demands not only physical reinforcement but also regulatory instruments capable of steering consumer behavior toward grid-compatible operation.

This thesis develops a comparative optimization framework to assess how different tariff schemes influence both user-side investment decisions and network development. The model integrates a detailed Distribution Network Expansion Planning (DNEP) formulation with Prosumer Energy System (PES) models. Two coordination regimes are compared: a centralized benchmark, where a social planner co-optimizes all assets to minimize total system cost, and a decentralized configuration, where prosumers act independently to minimize their own bills while the Distribution System Operator (DSO) reinforces the grid to ensure its safe operation.

By contrasting these two regimes, the framework identifies how various tariff structures guide decentralized decisions relative to the system-wide optimum. Results demonstrate that tariff design decisively shapes grid evolution and prosumer strategies, but its effectiveness is strongly context-dependent, influenced by technological costs and resource availability.

Contents

List of Figures

List of Tables

List of Acronyms

AC	Alternating Current	**ACER**	Agency for the Cooperation of Energy Regulators
CAPEX	Capital Expenditure	**CDF**	Cumulative Distribution Function
DC	Direct Current	**DG**	Distributed Generation
DNEP	Distribution Network Expansion Planning	**DSO**	Distribution System Operator
EC	European Commission	**EHP**	Electric Heat Pump
ESS	Energy Storage System	**EV**	Electric Vehicle
GHG	Greenhouse Gas	**HV**	High Voltage
IPCC	Intergovernmental Panel on Climate Change	**LCT**	Low-Carbon Technology
LV	Low Voltage	**MILP**	Mixed-Integer Linear Programming
MINLP	Mixed-Integer Non-Linear Programming	**MST**	Minimum Spanning Tree
MV	Medium Voltage	**OPEX**	Operational Expenditure
PES	Prosumer Energy System	**PV**	Photovoltaic
SOC	State of Charge	**STATCOM**	Static Synchronous Compensator
TFC	Total Final Consumption	**TSO**	Transmission System Operator

Notation Summary

Sets

$p \in \mathscr{P}$	Discrete time steps	$b \in \mathscr{B}$	Load buses
$s_{hv} \in \mathscr{S}_{HV}$	HV substations	$s_{mv} \in \mathscr{S}_{MV}$	MV substations
$c \in \mathscr{C}$	Conductor types	$l_{ij} \in \mathscr{L}$	Candidate power lines
$l_k \in \mathscr{L}_k^{\text{to/from}}$	Lines to/from bus k	$l_{s_{mv}} \in \mathscr{L}_{s_{mv}}^{\text{to/from LV}}$	LV lines to/from s_{mv}
$j \in \mathscr{J}$	All nodes ($\mathscr{B} \cup \mathscr{S}_{HV} \cup \mathscr{S}_{MV}$)		

Parameters

$P_{load,p,b}$	Active power demand at bus b, period p [MW]	$Q_{load,p,b}$	Reactive power demand at bus b, period p [Mvar]
I_p	Solar irradiance at period p [MW/m^2]	$r_{l,c}$	Resistance of line l with conductor c [kΩ]
$x_{l,c}$	Reactance of line l with conductor c [kΩ]	$I_{max,c}$	Max current rating of conductor c [kA]
V_{min}	Minimum voltage [V]	V_{max}	Maximum voltage [V]
A_b^{max}	Max PV installation at bus b [m^2]	$\pi_{s_{hv}}$	HV substation capacity cost [k€/MVA]
$\pi_{s_{mv}}$	MV substation capacity cost [k€/MVA]	$\pi_{statcom}$	Statcom capacity cost [k€/Mvar]
π_{pv}	PV capacity cost [k€/m^2]	$\pi_{storage}$	Storage capacity cost [k€/kWh]
$\pi_{inverter}$	Inverter capacity cost [k€/kVA]	$f_{s_{hv}}$	HV substation installation cost [k€]
$f_{s_{mv}}$	MV substation installation cost [k€]	$f_{statcom}$	Statcom installation cost [k€]
f_{pv}	PV installation cost [k€]	$f_{storage}$	Storage installation cost [k€]
$f_{inverter}$	Inverter installation cost [k€]	π_{import}	Energy import cost [k€/MWh]
π_{export}	Energy export cost [k€/MWh]	π_{losses}	Energy losses cost [k€/MWh]
$\eta_{storage}$	Storage efficiency		

Variables

α_l	Line l activation	$\delta_{l,c}$	Conductor c choice in line l
$\beta_{s_{hv}}$	HV substation s_{hv} activation	$\gamma_{s_{mv}}$	MV substation s_{mv} activation
μ_b	Statcom at bus b activation	$S_{s_{hv}}$	HV substation s_{hv} capacity [MVA]
$S_{s_{mv}}$	MV substation s_{mv} capacity [MVA]	$Q_{Statcom_b}$	Statcom at bus b capacity [Mvar]
π_b	PV installation at bus b option	σ_b	Storage installation at bus b option

$A_{pv,b}$	PV capacity at bus b [m^2]	$S_{inv,b}$	Inverter capacity at bus b [kVA]
$E_{stor,b}$	Storage capacity at bus b [kWh]	$P_{p,l}$	Active power flow in line l at period p [MW]
$Q_{p,l}$	Reactive power flow in line l at period p [Mvar]	$i^2_{p,l}$	Current squared in line l at period p [kA]
$P_{p,l,c}$	Active power flow divided by conductor c [MW]	$Q_{p,l,c}$	Reactive power flow divided by conductor c [Mvar]
$i^2_{p,l,c}$	Current squared divided by conductor c [kA]	$v^2_{p,j}$	Voltage squared at node j [V]
$P_{p,s_{mv}}$	Active power flow through MV substation s_{mv} at period p [MW]	$Q_{p,s_{mv}}$	Reactive power flow at MV substation s_{mv} at period p [Mvar]
$P_{p,s_{hv}}$	Active power flow through HV substation s_{hv} at period p [MW]	$Q_{p,s_{hv}}$	Reactive power flow at HV substation s_{hv} at period p [Mvar]
$Q_{statcom,p,b}$	Reactive power produced by statcom at bus b at period p [Mvar]	$\Delta i^2_{p,l,c}$	Overcurrent slack for line l, conductor c, period p [kA]
$P_{bus,p,b}$	Net active power injection at bus b, period p [MW]	$Q_{bus,p,b}$	Net reactive power injection at bus b, period p [Mvar]
$P_{pv,p,b}$	PV production at bus b, period p [kW]	$E_{p,b}$	Storage energy at bus b, period p [kWh]
$P_{ch,p,b}$	Storage charging power at bus b, period p [kW]	$P_{dis,p,b}$	Storage discharging power at bus b, period p [kW]
$P_{inv,p,b}$	Inverter active power at bus b, period p [kW]	$Q_{inv,p,b}$	Inverter reactive power at bus b, period p [kvar]
$\hat{\gamma}_{s_{mv}}$	MV substation s_{mv} topology activation	F_l	Fictitious power flow in line l
$F_{unserved,b}$	Unserved fictitious power at bus b	$F_{s_{hv}}$	Fictitious power capacity of HV substation s_{hv}

Chapter 1

Introduction

1.1 The Dual Imperative: Climate Action and Energy Sovereignty

Europe's energy paradigm is being fundamentally reshaped by a dual imperative. The first is the unequivocal scientific consensus on the necessity of mitigating climate change driven by anthropogenic greenhouse gas (GHG) emissions [1]. This environmental mandate is not merely a policy objective but a societal demand, with a clear majority of European Union (EU) citizens recognizing climate action as an urgent priority [2]. The second imperative is the pursuit of energy security and sovereignty. The systemic vulnerabilities of a fossil-fuel-dependent economy have been starkly exposed by recent geopolitical instabilities, demonstrating that the transition to local, renewable energy sources is a matter of strategic autonomy as much as it is one of environmental stewardship [3]. Embracing the energy transition is, therefore, a challenge the EU must confront to secure both its environmental and geopolitical future.

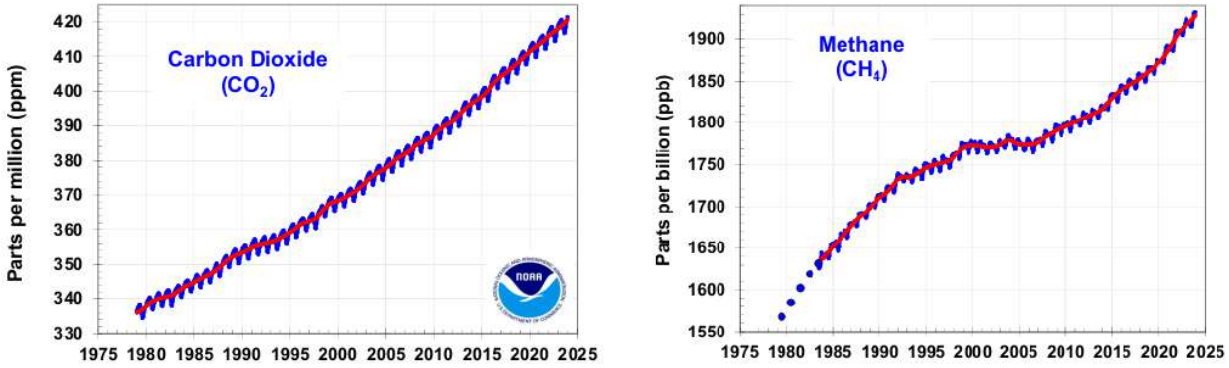

Figure 1.1: Atmospheric concentrations of CO_2 and CH_4 continue to rise at an accelerating pace, as shown by data from [4, 5]. This persistent trend highlights the challenge of current climate mitigation efforts, which have not yet been sufficient to slow the rate of GHG accumulation.

1.1.1 Europe's Strategy: Electrification as the Leading Pathway

In response to this dual challenge, the European Union has established an ambitious policy framework: the European Green Deal and the REPowerEU plan have been translated into binding legislation through the European Climate Law and the revised Renewable Energy Directive (RED III). The EU is now committed to reducing GHG emissions by 55% by 2030 and achieving a 42.5% share of renewable energy in total final consumption [6, 7].

Reaching such targets requires not only replacing fossil fuels as primary energy sources but also as energy carriers. Among the possible technological pathways, electrification has emerged as the most viable and immediate option, enabling the direct use of renewable electricity in end-use sectors such as transport and heating through technologies like Electric Vehicles (EVs) and Electric Heat Pumps (EHPs). Alternative pathways, such as advanced biofuels and green hydrogen, still face significant hurdles in terms of technological maturity, scalability, and cost-competitiveness, making them less likely to contribute substantially to the 2030 targets [9, 10].

Crucially, this transition from molecules to electrons depends not only on top-down policy commitments but also on millions of decentralized investment decisions made by consumers and producers. For the transition to progress at the required pace, clear economic signals must guide households and businesses towards adopting new technologies. Instruments such as EV subsidies, tax credits for building efficiency, transparent tariff structures, and well-designed price signals are the key mechanisms that translate high-level EU targets into concrete investments, shaping consumer behavior and accelerating emission reductions.

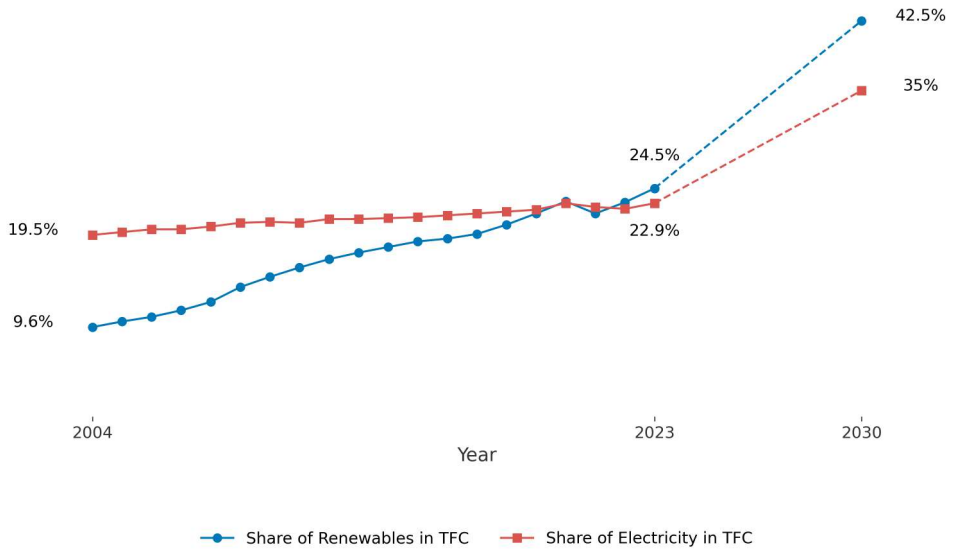

Figure 1.2: Evolution of energy shares in the EU's TFC. In the context of 2030 climate goals we highlight the necessary trend to reach the binding 42.5% renewable energy target and the projected 35% of electrification required to reach such target.

1.2 Distribution Networks: The Primary Bottleneck and Opportunity

As Europe pursues an electrification-led strategy, local distribution networks (DNs) are rapidly becoming the primary bottleneck. Historically designed for unidirectional power flow from large, central power stations to passive consumers, these networks are ill-equipped for the demands of a decarbonized energy system. The mass adoption of distributed energy resources and new electric loads creates a threefold challenge:

1. **Increased Peak Demand:** The simultaneous charging of EVs or operation of EHPs during cold spells can create new, highly localized demand peaks, potentially exceeding the capacity of existing infrastructure. Figure 1.3a shows how Italian Distribution System Operator (DSO) is forecasting a increase of peak consumption up to 30% for some regions.

2. **Reverse Power Flows:** The proliferation of rooftop solar Photovoltaic systems (PV) introduces bidirectional energy flows that can overwhelm local transformers and violate voltage limits. (Figure 1.3b) proves how this phenomenon spread in conjunction with the proliferation of solar panels and how is currently affecting 29% of the HV / MV grid infrastructure for at least 5% of the time.

3. **New Consumption Patterns:** Weather-dependent renewable generation and new consumption habits introduce a level of variability that legacy infrastructure was not designed to manage. Figure 1.3c illustrates the magnitude of this phenomenon: under specific operating conditions, the total power flowing into the Italian DNs has been halved in less than 15 years. Most notably, this curve now exhibits a pronounced sensitivity to meteorological variations at the local scale.

The scale of required physical upgrades is daunting, with investment needs for DNs estimated at €400–€600 billion by 2030 to avoid stalling the energy transition [11]. However, the challenge is not merely financial but technological. Relying on brute-force reinforcement with more copper and steel is an inefficient strategy that fails to address the grid's operational dynamics. A more intelligent approach is needed—one that increases the grid's hosting capacity through transparent price signals, markets for ancillary services, and tariffs that reward flexible consumption. The key to this transformation lies in the inherent capabilities of the assets themselves: EVs, batteries, and heat pumps can be shifted from being part of the problem to being the core of the solution.

A lot of the tex

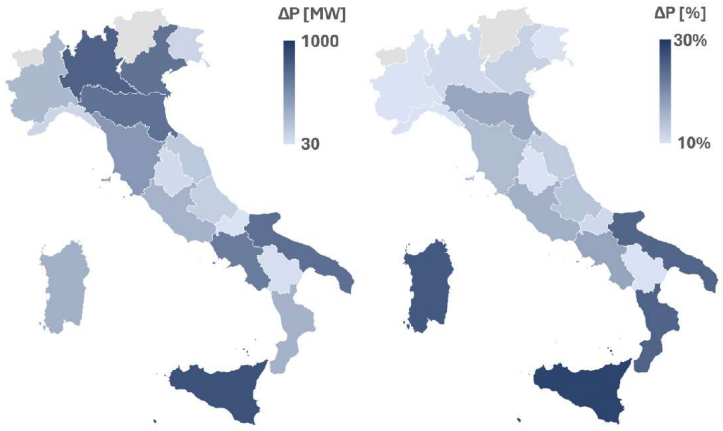

(a)

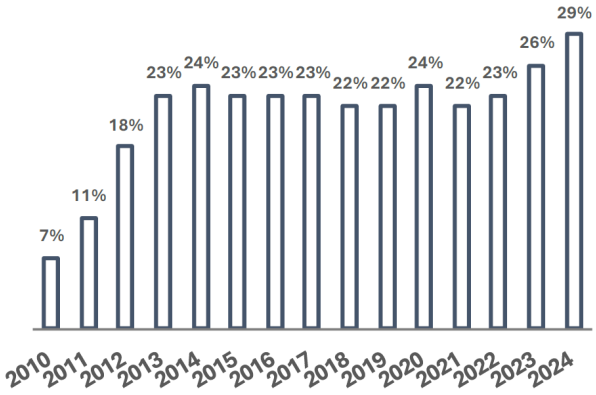

(b)

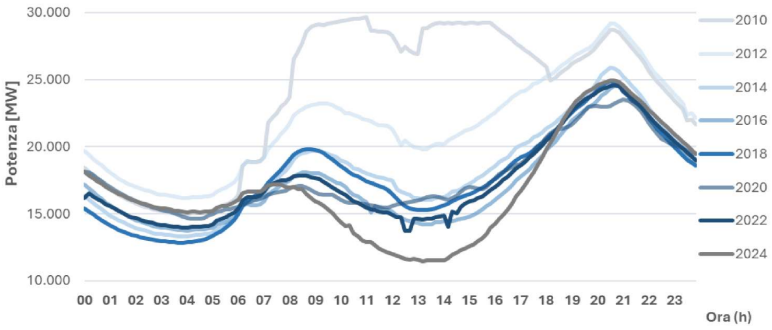

(c)

Figure 1.3: State of the Italian distribution grid as described in the DSO annual report [12]:
(a) Estimate of the absolute and percentage increase in maximum power 2029 vs 2024.
(b) HV/MV sections that experienced reversal of energy flow for more than 5% of the time.
(c) Trend of the total power flow from the NTG to the E-Distribuzione network on a typical weekday in August.

Chapter 2

Literature Review

2.1 The Evolving Paradigm of Distribution Network Expansion Planning

Distribution Network Expansion Planning (DNEP) is the primary framework used to determine the most economically efficient strategy for reinforcing the grid. The core task of DNEP is to select the grid upgrades necessary to serve a forecasted future demand while respecting all technical constraints. As comprehensively detailed in [13], this framework can be implemented in a variety of different ways: the demand forecast can range from deterministic worst-case scenarios [14] to complex probabilistic models accounting for multiple investment stages [15], additionally the portfolio of available grid upgrades can be limited to specific technologies or broader: in the past, these upgrades were limited to conventional grid assets such as the installation or reinforcement of lines and substations [16], while in the last decade, as the energy transition has driven a significant evolution of the field, DNEP models have routinely incorporated Low-Carbon Technologies (LCTs) as investment alternatives, including the optimal sizing and siting of Distributed Generation (DG) and Energy Storage Systems (ESSs) [17] but also of EV charging infrastructure [18, 19]. More recently, the paradigm has begun to shift again to include non-wire alternatives, which use the intelligent operation of flexible resources to defer costly physical upgrades, in this regard [20] considers the possibility to use inverters for grid support, while [21] evaluates the cost-effectiveness of these solution when compared to traditional grid reinforcements. Depending on the scope of the program and the modeling choices made, the problem's complexity can vary, thus, solution techniques range from exact optimization methods [22] to heuristic methods such as genetic [23] and constructive [25] algorithms or particle swarm optimization [24].

2.2 The Regulatory Pivot to Economic Instruments

The DNEP literature demonstrates a technical potential for finding highly efficient system solutions by co-optimizing network assets, LCTs, and non-wire strategies. However, many of these advanced models are formulated from the perspective of a single, centralized planner with control over all assets. This approach conflicts with the EU's regulatory reality, where DSOs are prohibited from owning and operating generation or storage assets [26]. In fact, The European regulatory body, the Agency for the Cooperation of Energy Regulators (ACER), defines price signal as the DSO's tool for steering network users towards patterns that incentivize grid-friendly behavior, enhance system-wide efficiency and postpone the need for expensive grid reinforcements [27]. The challenge, therefore, is how to design price signals that effectively steer decentralized network users towards the system-wide efficiencies identified by centralized optimization models. To address this, recent research has increasingly turned to game-theory and market-based modeling approaches to represent how DSOs can influence network users through indirect mechanisms rather than direct control. In particular, game-theoretic formulations have been used to model interactions between the DSO and owners of distributed generation through a Stackelberg game [28]. This formulation was later extended to represent prosumers as strategic agents capable of optimizing both their consumption and generation decisions within the same hierarchical framework [29]. Finally, market-based environments have been employed both to simulate the procurement of flexibility services [30] and to analyze their potential failures [31].

Chapter 3

Methodology

3.1 Core Analytical Method: The Comparative Scenarios

Building on the presented body of work, the objective of this thesis is to develop a tool to evaluate how tariff structure influence grid development. In particular we are interested in identifying which economic signals most effectively drive users toward cost efficient behavior and in what this behavior is. The analysis is based on a comparison between two coordination regimes:

- Centralized benchmark: a social planner co-optimizes all investments and operations—both grid and user-side assets—to minimize total system cost. This represents the theoretical efficiency frontier under perfect coordination.
- Decentralized configuration: the DSO defines the tariff parameters, after which each user independently minimizes its electricity bill by optimally investing in and operating local technologies. The resulting power exchange profiles determine the network reinforcements that the DSO must implement to ensure feasibility.

Comparing the total system cost of these two scenarios quantifies the degree of coordination achieved under a given tariff. This formulation enables a direct and quantitative assessment of the synchronization ability of tariff signals—that is, their capacity to align decentralized economic decisions with overall system efficiency.

3.2 Test Case Definition: The Campus Dataset

To demonstrate the proposed framework, we apply it to a dataset of synthetic campuses Fig 3.1 that emulate realistic distribution network layouts. Each campus spans a maximum area of ap-

proximately 9 km^2, it is comprised of four districts, and comprises between 35 and 55 load buses, which collectively reach a peak power demand between 3 and 5 MW.

The dataset includes a primary substation and several load buses, each characterized by geographical coordinates and voltage level (medium or low). For the load buses, hourly active and reactive power profiles are also provided. Moreover, the combination of the solar irradiance vector and the available surface area (A_b^{max}) at each bus determines its photovoltaic potential.

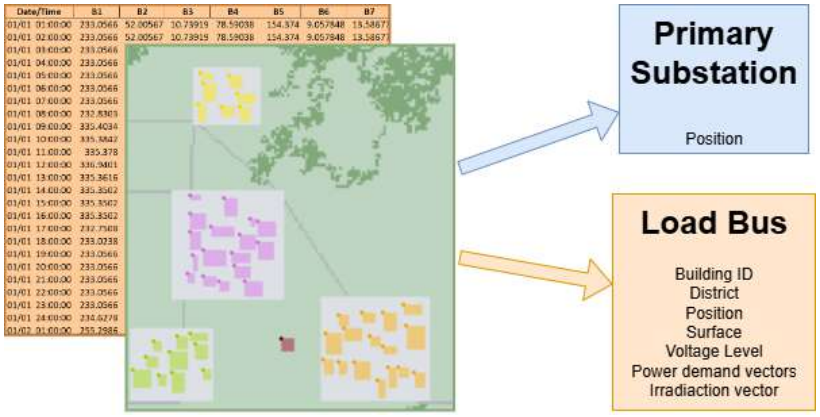

Figure 3.1: Structure of the Campus dataset. The data for each campus include an interactive map defining geographical and district boundaries, and a file containing the annual time series for demand and irradiance.

The study adopts a greenfield planning approach, designing the network from scratch to isolate the economic and operational impacts of tariff design from legacy infrastructure effects. This enables a transparent comparison between centralized and decentralized scenarios

To allow the optimization model to design a complete and technically feasible network, the dataset is augmented with candidate options for key assets:

- **Secondary substations:** Within each district, three candidate locations are randomly generated as potential MV/LV substations. The model determines which of these are built as part of the optimal solution.

- **Conductors:** A catalog of available conductor types is defined, covering a broad range of capacities and costs. This enables both short LV connections and higher-capacity MV feeders. The properties of the available conductors are summarized in Table 3.1.

- **Candidate lines:** All possible interconnections between nodes are initially considered, forming a complete graph. This full set guarantees that the optimal network topology lies within the feasible space and provides a reference benchmark for subsequent spatial reduction methods.

Conductors	q **[mm^2]**	r **[Ω/km]**	x_l **[Ω/km]**	i_{max} **[kA]**	**Cost [k€/km]**
Poppy	53.50	0.5502	0.429	0.23	100
Oxlip	107.30	0.2747	0.402	0.34	120
Daisy	135.30	0.2180	0.394	0.46	150
Tulip	170.60	0.1732	0.381	1.53	200
Billy	300.00	0.0900	0.190	3.00	280

Table 3.1: Properties of Different Conductors Used in the Campus Test Case

3.3 Applications and Interpretation of Results

The quantification of the Total System Cost Gap, derived from the comparative scenarios, can be used as a foundation for several applications. It provides a tangible metric that indirectly measures the costs associated with sub-optimal capital allocation, inefficient LCT control strategies, and misaligned economic signals under decentralized decision-making. This enables three key insights:

1. **Engineering Better Tariffs:** The most direct application is the ability to test and compare different tariff structures. A tariff that results in a smaller Total System Cost Gap is, by definition, more effective at incentivizing efficient system-wide behavior. This allows for evidence-based tariff design. The framework does not directly optimize tariff structures but rather assesses their effectiveness by measuring the coordination gap they induce.

2. **Evaluating LCT Control Strategies:** The framework can be used to assess how different operational strategies for LCTs, particularly within the decentralized scenario, impact the overall system cost gap. This provides insights into best practices for consumer-level energy management.

3. **Informing the Pricing of Flexibility:** The framework provides a powerful benchmark for valuing flexibility and ancillary services. The cost of grid reinforcements that are deferred or avoided thanks to flexible resources (like LCTs providing demand response or storage services) represents the upper bound on the economic value of those services. The model can thus be used to establish a rational basis for the price of flexibility procured by the DSO in local markets.

Chapter 4

Mathematical Formulation

In this chapter, we define and describe the optimization models that form the analytical foundation of this work. The problem is structured around two complementary formulations: the Distribution Network Expansion Planning (DNEP) model and the Prosumer Energy System (PES) model. The first represents the DSO perspective; it is responsible for grid investment and its correct functioning, while the second models the decentralized behavior of network users who invest in and operate distributed assets.

4.1 Distribution Network Expansion Planning (DNEP)

The DNEP model determines the optimal reinforcement and operation strategy for the distribution grid over a defined planning horizon. Its objective (M1–1), is to minimize the total annualized system cost. This is composed by four cost components, defined in block (M1–2): the grid investment cost C_{grid}, the cost of imported electricity at the HV substation C_{import}, the revenues collected from end-users through network tariffs $C_{revenue}$, and the penalty term C_{pen} applied to operational or topological violations.

The grid investment cost represents the annualized capital expenditure associated with all grid components, including the installation and capacity costs of high- and medium-voltage substations, the installation of conductors of various types, and the investment in reactive power compensating devices such as STATCOMs while the import cost accounts for the energy purchased from the upstream transmission system.

The revenue term reflects the payments collected from consumers based on their electricity consumption and the adopted tariff structure. As tariffs are exogenously defined, this term does not represent a decision variable of the optimization but rather a fixed quantity that offsets part of the total system cost. Finally, the penalty cost aggregates the slack variables introduced to maintain model feasibility, such as overcurrent or unserved power flow terms. It is multiplied by a

large weighting coefficient, ensuring that any violation of the physical or operational constraints is heavily penalized. This term is not a real expense as it must be strictly zero for the solution to be accepted.

The model's physical behavior is described by the DistFlow equations (M1–3), which link active and reactive power flows to current magnitudes and node voltages. These equations capture the non-linear electrical relationships governing radial distribution feeders. To maintain realistic operating conditions, the operational constraints (M1–4) bound the voltage magnitude at every bus within the admissible range and ensure that the current on each line does not exceed the thermal limit of its conductor. In addition, the voltage at each active HV substation is fixed at 1 p.u. to provide a reference for the network.

The Asset Investment and Logic block (M1–5) integrates binary investment variables with the physical constraints of the system. Binary variables determine whether each line, substation, or compensating device is built, and which conductor type is selected. This block ensures that physical limits, such as the maximum current of a selected conductor or the quadratic capacity of substations, are only enforced when the corresponding asset is installed. It also aggregates per-conductor flows into total line flows and total current magnitudes.

The Nodal Power Balance equations (M1–6) implement Kirchhoff's Current and Power Laws for every node type (HV, MV, and load buses). They ensure that the algebraic sum of inflows and outflows of active and reactive power equals the local net injection, thereby maintaining energy conservation across the entire grid.

Finally, the Network Topology constraints (M1–7) ensure that the optimized grid configuration is both connected and radial. The connectivity requirement arises from the presence of distributed energy resources: in principle, local generation could fully supply certain areas, leading to feasible yet electrically disconnected solutions. To prevent this, a fictitious power flow is introduced. Each load bus is modeled as consuming a fixed unit of this artificial commodity, while only HV substations are allowed to produce it as described by balance constraints (M1–7a–c). Furthermore, it is necessary to constraint fictitious power to only flow in built lines (M1-7d).

To enforce radiality, an additional topological condition is imposed: the number of active lines must equal the total number of active nodes minus one. Since the number of substations to be built is not known a priori, the model dynamically counts as active only those substations connected by at least one line, as enforced by constraint (M1–7f). Together, these relationships guarantee that the resulting configuration forms a single spanning tree, fully connected and free of loops, consistent with the operational structure of real distribution networks.

DNEP Model Formulation

Objective Function:

$$\min\ C_{grid} + C_{import} - C_{revenue} + C_{pen} \tag{M1-1}$$

Cost Definitions:

$$C_{grid} = \frac{1}{T_{horizon}} \left(C_{lines} + C_{HVsub} + C_{MVsub} + C_{Statcom}\right) \tag{M1-2a}$$

$$C_{lines} = \sum_{l,c} \delta_{l,c} \pi_{l,c} \tag{M1-2b}$$

$$C_{HVsub} = \sum_{s_{hv}} (S_{s_{hv}} \pi_{s_{hv}} + \beta_{s_{hv}} f_{s_{hv}}) \tag{M1-2c}$$

$$C_{MVsub} = \sum_{s_{mv}} (S_{s_{mv}} \pi_{s_{mv}} + \gamma_{s_{mv}} f_{s_{mv}}) \tag{M1-2d}$$

$$C_{Statcom} = \sum_{b} (Q_{Statcom_b} \pi_{Statcom} + \mu_{Statcom_b} f_{Statcom_b}) \tag{M1-2e}$$

$$C_{import} = \sum_{p,s_{hv}} P_{p,s_{hv}} \cdot \pi_{import} \tag{M1-2f}$$

$$C_{revenue} = \sum_{b} f(P_{bus,p,b}, Q_{bus,p,b}) \tag{M1-2g}$$

$$C_{pen} = C_{penalty} \cdot \left(\sum_{p,l,c} \Delta i^2_{p,l,c} + \sum_{b} F_{unserved,b} \right) \tag{M1-2h}$$

Power Flow (DistFlow):

$$v^2_{p,j} - v^2_{p,i} = -2 \sum_{c} (r_{l,c} P_{p,l,c} + x_{l,c} Q_{p,l,c}) + (r^2_{l,c} + x^2_{l,c}) i^2_{p,l,c} \qquad \forall p,\ l = (i,j) \mid \alpha_l = 1 \tag{M1-3a}$$

$$v^2_{p,i}\, i^2_{p,l} \geq P^2_{p,l} + Q^2_{p,l} \qquad \forall p,\ l = (i,j) \tag{M1-3b}$$

$$Loss_{p,l} = \sum_{c} r_{l,c}\, i^2_{p,l,c} \qquad \forall p, l \tag{M1-3c}$$

Operational Limits:

$$V^2_{min} \leq v^2_{p,j} \leq V^2_{max} \qquad \forall p,\ j \in \mathscr{B} \cup \mathscr{S}_{MV} \tag{M1-4a}$$

$$i^2_{p,l,c} - \Delta i^2_{p,l,c} \leq I^2_{max,c} \cdot \delta_{l,c} \qquad \forall p, l, c \tag{M1-4b}$$

$$v^2_{p,s_{hv}} = 1 \qquad \forall p, s_{hv} \mid \beta_{s_{hv}} = 1 \tag{M1-4c}$$

Asset Investment & Logic:

$$\alpha_l = \sum_{c \in \mathscr{C}} \delta_{l,c} \qquad \forall l \tag{M1-5a}$$

$$|P_{p,l,c}| \leq \delta_{l,c} I_{max,c} V_{max} \qquad \forall p, l, c \tag{M1-5b}$$

$$|Q_{p,l,c}| \leq \delta_{l,c} I_{max,c} V_{max} \qquad \forall p, l, c \tag{M1-5c}$$

$$P_{p,l} = \sum_{c \in \mathscr{C}} P_{p,l,c}, \quad Q_{p,l} = \sum_{c \in \mathscr{C}} Q_{p,l,c}, \quad i^2_{p,l} = \sum_{c \in \mathscr{C}} i^2_{p,l,c} \qquad \forall p, l \qquad \text{(M1-5d)}$$

$$\beta_{s_{hv}} S^2_{s_{hv}} \geq P^2_{p,s_{hv}} + Q^2_{p,s_{hv}} \qquad \forall p, s_{hv} \qquad \text{(M1-5e)}$$

$$\gamma_{s_{mv}} S^2_{s_{mv}} \geq P^2_{p,s_{mv}} + Q^2_{p,s_{mv}} \qquad \forall p, s_{mv} \qquad \text{(M1-5f)}$$

$$|Q_{Statcom,p,b}| \leq \mu_{Statcom_b} Q_{Statcom_b} \qquad \forall p, b \qquad \text{(M1-5g)}$$

Nodal Power Balance:

$$P_{p,s_{hv}} = \sum_{l \in \mathscr{L}^{from}_{s_{hv}}} P_{p,l} - \sum_{l \in \mathscr{L}^{to}_{s_{hv}}} (P_{p,l} - \sum_c r_{l,c} i^2_{p,l,c}) \qquad \forall p, s_{hv} \qquad \text{(M1-6a)}$$

$$Q_{p,s_{hv}} = \sum_{l \in \mathscr{L}^{from}_{s_{hv}}} Q_{p,l} - \sum_{l \in \mathscr{L}^{to}_{s_{hv}}} (Q_{p,l} - \sum_c i^2_{p,l,c} x_{l,c}) \qquad \forall p, s_{hv} \qquad \text{(M1-6b)}$$

$$0 = \sum_{l \in \mathscr{L}^{from}_{s_{mv}}} P_{p,l} - \sum_{l \in \mathscr{L}^{to}_{s_{mv}}} (P_{p,l} - \sum_c r_{l,c} i^2_{p,l,c}) \qquad \forall p, s_{mv} \qquad \text{(M1-6c)}$$

$$0 = \sum_{l \in \mathscr{L}^{from}_{s_{mv}}} Q_{p,l} - \sum_{l \in \mathscr{L}^{to}_{s_{mv}}} (Q_{p,l} - \sum_c i^2_{p,l,c} x_{l,c}) \qquad \forall p, s_{mv} \qquad \text{(M1-6d)}$$

$$P_{p,s_{mv}} = \sum_{l \in \mathscr{L}^{fromLV}_{s_{mv}}} P_{p,l} - \sum_{l \in \mathscr{L}^{toLV}_{s_{mv}}} (P_{p,l} - \sum_c r_{l,c} i^2_{p,l,c}) \qquad \forall p, s_{mv} \qquad \text{(M1-6e)}$$

$$Q_{p,s_{mv}} = \sum_{l \in \mathscr{L}^{fromLV}_{s_{mv}}} Q_{p,l} - \sum_{l \in \mathscr{L}^{toLV}_{s_{mv}}} (Q_{p,l} - \sum_c i^2_{p,l,c} x_{l,c}) \qquad \forall p, s_{mv} \qquad \text{(M1-6f)}$$

$$P_{bus,p,b} = \sum_{l \in \mathscr{L}^{from}_{b}} P_{p,l} - \sum_{l \in \mathscr{L}^{to}_{b}} (P_{p,l} - \sum_c r_{l,c} i^2_{p,l,c}) \qquad \forall p, b \qquad \text{(M1-6g)}$$

$$Q_{bus,p,b} = Q_{statcom,p,b} + \sum_{l \in \mathscr{L}^{from}_{b}} Q_{p,l} - \sum_{l \in \mathscr{L}^{to}_{b}} (Q_{p,l} - \sum_c i^2_{p,l,c} x_{l,c}) \qquad \forall p, b \qquad \text{(M1-6h)}$$

Network Topology & Radiality:

$$1 - F_{unserved,b} = \sum_{l \in \mathscr{L}^{to}_{b}} F_l - \sum_{l \in \mathscr{L}^{from}_{b}} F_l \qquad \forall b \qquad \text{(M1-7a)}$$

$$F_{s_{hv}} = \sum_{l \in \mathscr{L}^{from}_{s_{hv}}} F_l - \sum_{l \in \mathscr{L}^{to}_{s_{hv}}} F_l \qquad \forall s_{hv} \qquad \text{(M1-7b)}$$

$$0 = \sum_{l \in \mathscr{L}^{to}_{s_{mv}}} F_l - \sum_{l \in \mathscr{L}^{from}_{s_{mv}}} F_l \qquad \forall s_{mv} \qquad \text{(M1-7c)}$$

$$|F_l| \leq \alpha_l |\mathscr{B}| \qquad \forall l \qquad \text{(M1-7d)}$$

$$\sum_{l \in \mathscr{L}} \alpha_l = \sum_{b \in \mathscr{B}} 1 + \sum_{s_{hv} \in \mathscr{S}_{hv}} \beta_{s_{hv}} + \sum_{s_{mv} \in \mathscr{S}_{mv}} \hat{\gamma}_{s_{mv}} - 1 \qquad \text{(M1-7e)}$$

$$\hat{\gamma}_{s_{mv}} \leq \sum_{l \in \mathscr{L}_{s_{mv}}} \alpha_l \qquad \forall s_{mv} \qquad \text{(M1-7f)}$$

4.2 Prosumer Energy System (PES)

The PES model determines the optimal investment and operational strategy for distributed assets installed at each load bus. Each prosumer can invest in PV panels, battery energy storage, and inverter capacity to partially supply its own demand and exchange electricity with the grid under a given tariff structure. The objective of the model, defined in (M2), is to minimize the total annualized cost, which includes both the investment and installation cost of the selected assets (M2–2a) and the cost of electricity (M2–2e), computed as a function of the net exchanged power and the applicable tariff.

Each prosumer is represented by a simplified two-bus configuration. The DC bus hosts the PV generation and the energy storage system, while the AC bus connects to the grid and supplies the local load. A single inverter connects the two sides, enabling bidirectional power exchange. The inverter can also control reactive power within its apparent power limits, contributing to local voltage support.

The operation of the system is governed by a set of constraints that ensure a consistent and physically meaningful representation of the energy flows. The AC bus power balance (M2–3) ensures that the power requested by the load is fed either from the inverter or from the grid. The PV generation constraints (M2–4) limit the installed panel area to the available surface and link the generated power to the local irradiance. The energy storage system constraints (M2–5) describe the temporal evolution of the battery's state of charge, accounting for charging and discharging efficiencies and enforcing a daily cyclic energy balance. Finally, the inverter and DC-side balance equations (M2–6) establish the relationship between the inverter's power exchange and its capacity, while ensuring the DC-side power balance between storage, PV generation, and conversion to or from the AC side.

Microgrid Model Formulation (for a single bus b)

Objective Function:

$$\min\ C_{asset,b} + C_{elec,b} \tag{M2-1}$$

Cost Definition:

$$C_{asset,b} = \frac{1}{T_{horizon}} \left(C_{PV,b} + C_{Storage,b} + C_{Inv,b} \right) \tag{M2-2a}$$

$$C_{PV,b} = A_{pv,b}\, \pi_{pv} + \pi_b\, f_{pv} \tag{M2-2b}$$

$$C_{Storage,b} = E_{stor,b}\, \pi_{storage} + \sigma_b\, f_{storage} \tag{M2-2c}$$

$$C_{Inv,b} = S_{inv,b}\,\pi_{inverter} \tag{M2-2d}$$

$$C_{elec,b} = f(P_{bus,p,b}, Q_{bus,p,b}) \tag{M2-2e}$$

Bus Power Balance (Load Side):

$$P_{bus,p,b} = P_{load,p,b} - P_{inv,p,b} \qquad \forall p \tag{M2-3a}$$

$$Q_{bus,p,b} = Q_{load,p,b} - Q_{inv,p,b} \qquad \forall p \tag{M2-3b}$$

PV System:

$$A_{pv,b} \leq A_b^{max} \cdot \pi_b \tag{M2-4a}$$

$$P_{pv,p,b} \leq A_{pv,b} \cdot I_p \cdot \eta_{pv} \qquad \forall p \tag{M2-4b}$$

Energy Storage System (ESS):

$$E_{stor,b} \leq E_{stor}^{max} \cdot \sigma_b \tag{M2-5a}$$

$$E_{p,b} \leq E_{stor,b} \qquad \forall p \tag{M2-5b}$$

$$E_{p,b} = E_{p-1,b} + \left(\eta_{stor} P_{ch,p,b} - \frac{1}{\eta_{stor}} P_{dis,p,b}\right) \Delta t \qquad \forall p : (p-1)\%24 \neq 0 \tag{M2-5c}$$

$$E_{p,b} = E_{p+23,b} \qquad \forall p : (p-1)\%24 = 0 \tag{M2-5d}$$

Inverter & DC Bus Balance:

$$S_{inv,b}^2 \geq P_{inv,p,b}^2 + Q_{inv,p,b}^2 \qquad \forall p \tag{M2-6a}$$

$$P_{pv,p,b} + P_{dis,p,b} = P_{inv,p,b} + P_{ch,p,b} \qquad \forall p \tag{M2-6b}$$

4.3 Decentralized and Centralized Coupling

The DNEP and PES formulations can be combined in two distinct ways, to obtain the two described degrees of coordination between network users and the DSO. For the decentralized formulation, the two models are solved sequentially. Each prosumer first solves its own PES optimization problem (M2), minimizing its individual cost under a given tariff scheme. This produces the net active and reactive power injections $(P_{bus,p,b}, Q_{bus,p,b})$, which represent the consumer interaction with the grid. These exchanges are then treated as fixed parameters within the DNEP problem (M1), which determines the least-cost grid reinforcement strategy that ensures operational feasibility under those user decisions.

This formulation mirrors the real-world regulatory setting in which prosumers act indepen-

dently while the DSO plans and operates the network based on their resulting demand and generation profiles. It captures how tariff structures shape user behavior and, in turn, how these decentralized decisions influence grid reinforcement needs and total system cost.

Conversely, for the centralized formulation, the two models are solved simultaneously within a single optimization problem. The coupling variables $P_{bus,p,b}$ and $Q_{bus,p,b}$ are no longer exchanged between separate problems but become endogenous decision variables jointly optimized alongside all grid and user-level variables. The objective function of the unified model is given by:

$$\min \left(C_{grid} + C_{import} - C_{revenue} + \sum_{b \in \mathscr{B}} (C_{asset,b} + C_{elec,b}) + C_{pen} \right). \tag{4.1}$$

Since the users' electricity payments are exactly equal to the DSO's revenues, the monetary exchange between the two sides cancels out from a system perspective. The objective thus simplifies to:

$$\min \left(C_{grid} + \sum_{b \in \mathscr{B}} C_{asset,b} + C_{import} + C_{pen} \right). \tag{4.2}$$

This formulation represents a fully coordinated, system-optimal scenario in which a central planner controls all grid and prosumer decisions simultaneously, internalizing every operational interaction. It provides a lower bound on the total system cost and serves as the reference for evaluating the efficiency loss that arises in the decentralized, tariff-driven case.

Chapter 5

Implementation

The DNEP model, as formulated in the previous chapter, is a Mixed-Integer Non-Linear Program (MINLP). Such problems are computationally demanding and cannot be solved directly for realistic network sizes. This chapter details the sequence of methodological steps implemented to transform the theoretical model into a tractable and operational framework.

We first introduce the linearization strategies used to convert the original MINLP into a Mixed-Integer Linear Program (MILP). We then present a scalability analysis performed on the linearized model to characterize its computational growth with respect to spatial and temporal dimensions. Successively, building on these insights, we apply a set of model reduction techniques—spatial pruning of candidate lines and temporal clustering of representative days—to manage complexity while preserving model accuracy. Finally, the chapter concludes with the validation of the resulting model against a non-linear power flow solver and the presentation of a heuristic developed to accelerate convergence on large-scale instances

5.1 Linearization of the MINLP Model

To render the DNEP formulation tractable, the first step involves its linearization—converting the original MINLP into a MILP through appropriate mathematical reformulations or approximations. This section describes the main non-linearities of the problem and the techniques used to address them, together with targeted experiments for evaluating their performance and tuning their parameters.

5.1.1 Linearization of the Absloute Value

A simple nonlinearity appears in constraints of the form $|x| \leq y$, which can be directly replaced by two linear inequalities:

$$x \leq y \tag{5.1}$$

$$x \geq -y \tag{5.2}$$

Together, these two constraints are exactly equivalent to the original nonlinear expression.

5.1.2 Polygonal Approximation of Circular Constraints

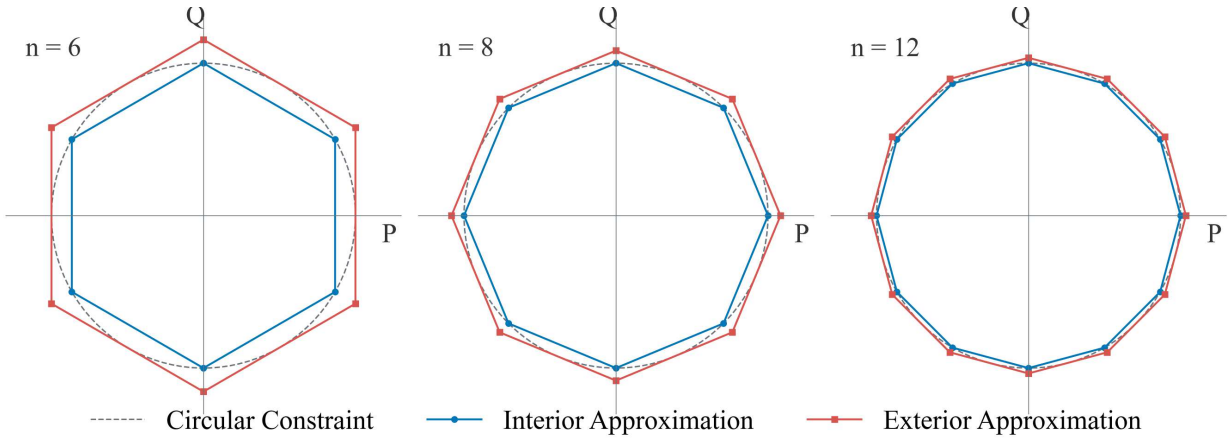

Figure 5.1: Graphic example of internal and external polygonal approximation

This technique linearizes the quadratic relationship $z^2 \geq x^2 + y^2$, which represents an asset rating constraint. The approach replaces the single quadratic inequality with N linear inequalities, approximating the circular feasible region by an N-sided regular polygon:

$$z \geq a_k x + b_k y \quad \forall k = 1, \ldots, N \tag{5.3}$$

where $a_k = \cos(2\pi k/N)$ and $b_k = \sin(2\pi k/N)$.

This outer polygonal approximation tends to overestimate the true feasible region, potentially resulting in an overestimation of the asset capacity. To ensure a conservative approximation, one that always satisfies the original non-linear constraint by remaining entirely within the circular boundary, the polygon is inscribed within the circle by scaling the constraints with a factor of $\cos(\pi/N)$. The resulting inner approximation is expressed as:

$$z \cdot \cos\left(\frac{\pi}{N}\right) \geq a_k x + b_k y \quad \forall k = 1, \ldots, N \tag{5.4}$$

The number of polygon sides N must be tuned to balance approximation accuracy and computational performance. To investigate this trade-off, we conducted an experiment comparing the proposed interior and exterior linearization with Gurobi's automatic handling of the original conic constraint. Gurobi can be configured to solve quadratic problems either through an outer-approximation scheme or by using continuous relaxations. Since the latter did not converge within several hours, our comparison focuses on the proposed linearization approaches and Gurobi's own linearized formulation based on outer approximation. The analysis therefore aims to quantify the trade-off between computational performance and solution precision among the viable linearization strategies.

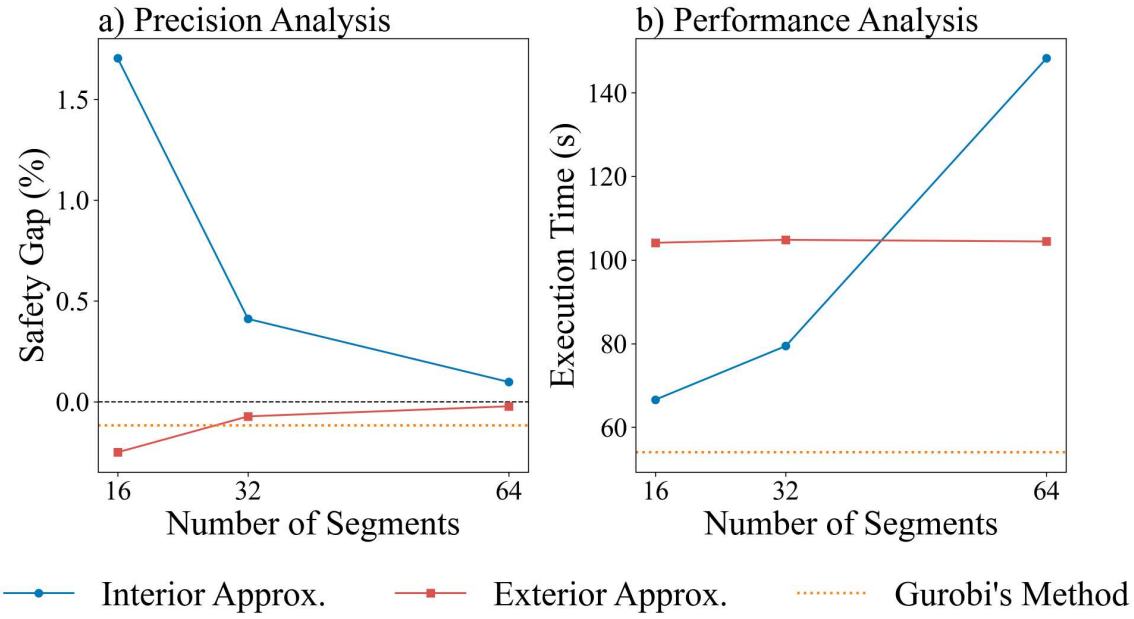

Figure 5.2: Time performance and precision of polygonal linearization, comparing the interior and exterior polygonal approximations using increasing number of segments with the automatic linearization performed by Gurobi.

The results, shown in Figure 5.2, illustrate the trade-off between computational cost, precision, and operational safety. Panel (a) highlights the essential safety difference: the proposed interior approximation consistently yields a positive Safety Gap, ensuring that the system's capacity is never overestimated. As the number of segments increases, precision improves and the approximation approaches the ideal zero-gap line from the conservative side. In contrast, both the exterior approximation and Gurobi's automatic method overestimate the asset's capacity and, thus, fail to enforce the original nonlinear constraint.

Panel (b) summarizes the performance trade-off. The increase in execution time is not strictly proportional to the number of segments but correlates with actual improvements in precision. In

other words, the computational cost rises noticeably only when the additional segments provide a tangible gain in accuracy. This behavior is particularly evident for the interior approximation, where the solver efficiently exploits the tighter feasible region, whereas the exterior approximation shows nearly constant solving times regardless of precision gains. As expected, Gurobi's built-in linearization remains the fastest overall, serving as a useful performance benchmark.

Overall, the proposed interior approximation provides a conservative and tunable solution that balances safety and precision. Although Gurobi achieves higher speed, its non-conservative nature introduces an operational risk, and its solver-specific implementation limits portability and tunability. By performing the linearization explicitly, the interior approach ensures solver-independent robustness and controllable precision, making it a reliable and generalizable choice.

5.1.3 Piecewise Linearization of the Square Function

Another key non-linearity arises from the complex power constraint: $v_{p,i}^2 \cdot i_{p,l}^2 \geq P_{p,l}^2 + Q_{p,l}^2$, it is important to note that in our model square of voltage and current variables are linear variables, in fact, the non linearity arises from the bilinear nature of this equation-the product between two variables-and from the square function applied to active and reactive power. To tackle this issue, a linearization based on the approximation of voltage and the picewise linearization of the square function is applied, this is implemented in the following steps:

1. **Approximating the voltage:** Since the admissible voltage range is narrow: $V \in [0.95; 1.05] p.u.$, we approximate its value to 1. Doing so removes the bilinear component of the equation that becomes: $i_{p,l}^2 \geq P_{p,l}^2 + Q_{p,l}^2$

2. **Obtaining the Absolute Power Value:** Power flow $P_{p,l}$ is decomposed into two non-negative components, $P_{p,l}^+$ and $P_{p,l}^-$, such that $P_{p,l} = P_{p,l}^+ - P_{p,l}^-$. The absolute value is their sum: $|P_{p,l}| = P_{p,l}^+ + P_{p,l}^-$. The same is done for reactive power $Q_{p,l}$

3. **Discretization of the Power Domain:** The continuous domain of absolute power, $[0, X_{max,l}]$, is partitioned into n contiguous segments, indexed by $d \in \mathscr{D}$.

4. **Defining Segment Lengths and Slopes:** The parameter $LPWB_{l,d}$ defines the width of each segment d. The slope of the approximating line for that segment, $SPWB_{l,d}$, is defined by the chord connecting the start and end points on the $f(x) = x^2$ curve:

$$SPWB_{l,d} = \frac{X_{end}^2 - X_{start}^2}{X_{end} - X_{start}} = X_{start} + X_{end} \tag{5.5}$$

5. **Formulating Linear Constraints:** The original non-linear inequality is replaced by a set of linear constraints using discretized power variables ($P_{p,l,d}, Q_{p,l,d}$):

$$|P_{p,l}| = \sum_{d \in \mathscr{D}} P_{p,l,d} \quad \text{and} \quad |Q_{p,l}| = \sum_{d \in \mathscr{D}} Q_{p,l,d} \tag{5.6}$$

$$0 \leq P_{p,l,d} \leq LPWB_{l,d} \quad \text{and} \quad 0 \leq Q_{p,l,d} \leq LPWB_{l,d} \tag{5.7}$$

$$i_{p,l}^2 \geq \sum_{d \in \mathscr{D}} SPWB_{l,d} \cdot P_{p,l,d} + \sum_{d \in \mathscr{D}} SPWB_{l,d} \cdot Q_{p,l,d} \tag{5.8}$$

The precision of this method strongly depends on how $LPWB_{l,d}$ is defined. To illustrate this, we compare two approaches: constant and logarithmic progression length.

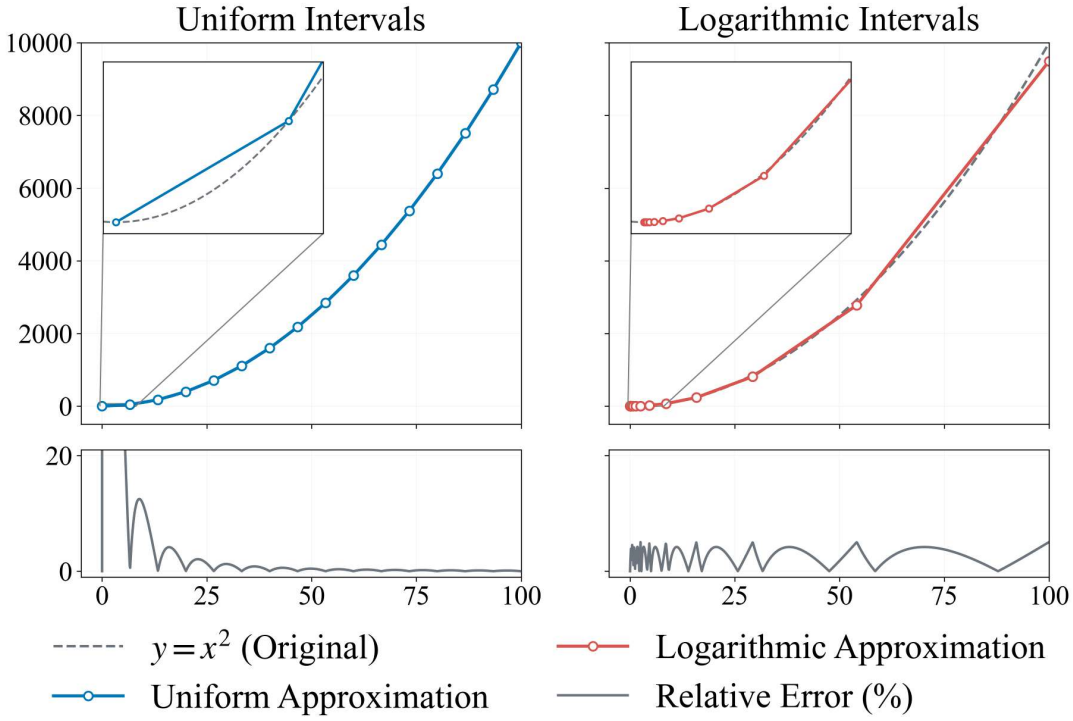

Figure 5.3: Example of piecewise linearization with constant and varying segment lengths, and the corresponding relative precision across the interval.

As shown in Fig. 5.3, the logarithmic method yields a more uniform relative error. To assess whether this improvement translates into higher overall precision and acceptable computational performance, we run the DNEP model for 24 time steps on a single district, varying only the linearization method.

Results in Fig. 5.4 show that the logarithmic segmentation achieves a relative error below 20%,

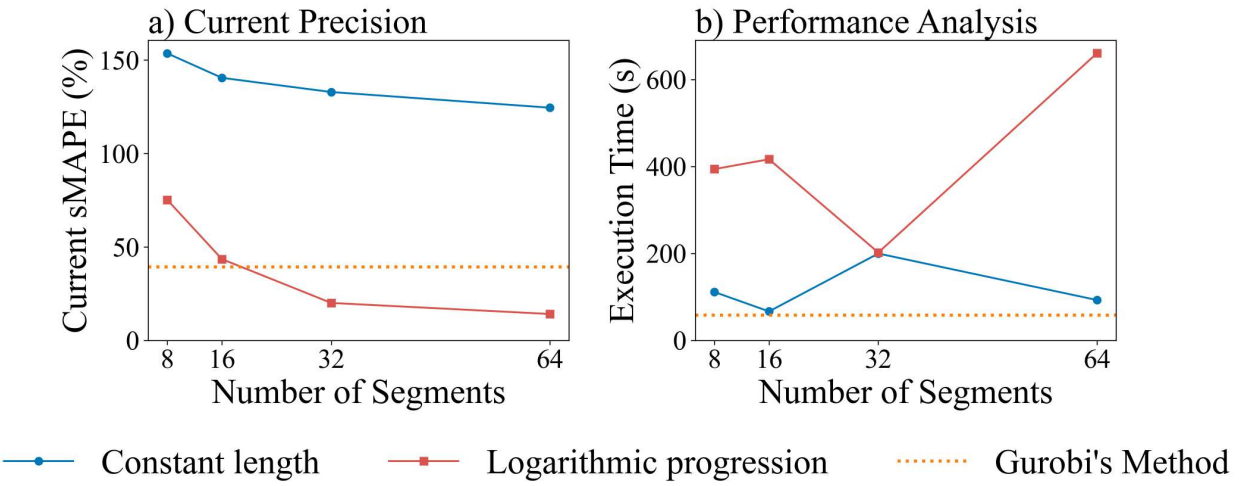

Figure 5.4: Computation time and precision of square-function linearization. Constant-length and logarithmic progression methods are compared with Gurobi's automatic linearization.

while the equal-segment method, although faster, remains above 120%. Notably, Gurobi's automatic linearization also struggles to reach satisfactory precision in this case.

5.1.4 Linearization of Indicator Constraints: The Big-M Method

Finally we linearize the logical "if-then" constraints, such as the DistFlow equations holding only for active lines ($\alpha_l = 1$). This is obtained by implementing the Big-M method. For an equality constraint like $g(x) = h(x)$, this consists in first decomposing the constraint into two inequalities: $g(x) \leq h(x)$ and $g(x) \geq h(x)$. Then we respectively add and subtract the Big-M term to the obtained inequalities. For the DistFlow voltage drop equation, this results in:

$$v_{p,j}^2 - v_{p,i}^2 \leq -2\sum_c (r_{l,c}P_{p,l,c} + x_{l,c}Q_{p,l,c}) + (r_{l,c}^2 + x_{l,c}^2)i_{p,l,c}^2 + M \cdot (1 - \alpha_l) \tag{5.9}$$

$$v_{p,j}^2 - v_{p,i}^2 \geq -2\sum_c (r_{l,c}P_{p,l,c} + x_{l,c}Q_{p,l,c}) + (r_{l,c}^2 + x_{l,c}^2)i_{p,l,c}^2 - M \cdot (1 - \alpha_l) \tag{5.10}$$

When $\alpha_l = 1$, the M terms become zero, enforcing the original equality. When $\alpha_l = 0$, the large M value makes the constraints non-binding.

5.2 Model Validation

The linearized model is validated against a nonlinear power flow solver based on the Newton–Raphson method. The network topology and net power exchanges obtained from the MILP optimization are

used as inputs to run the power flow analysis. The comparison between the two methods is shown in Figure 5.5. The close alignment of the points with the unity line confirms that the power flow results from the optimization are consistent with those from the nonlinear solver, thereby validating the adequacy of the adopted linear approximations.

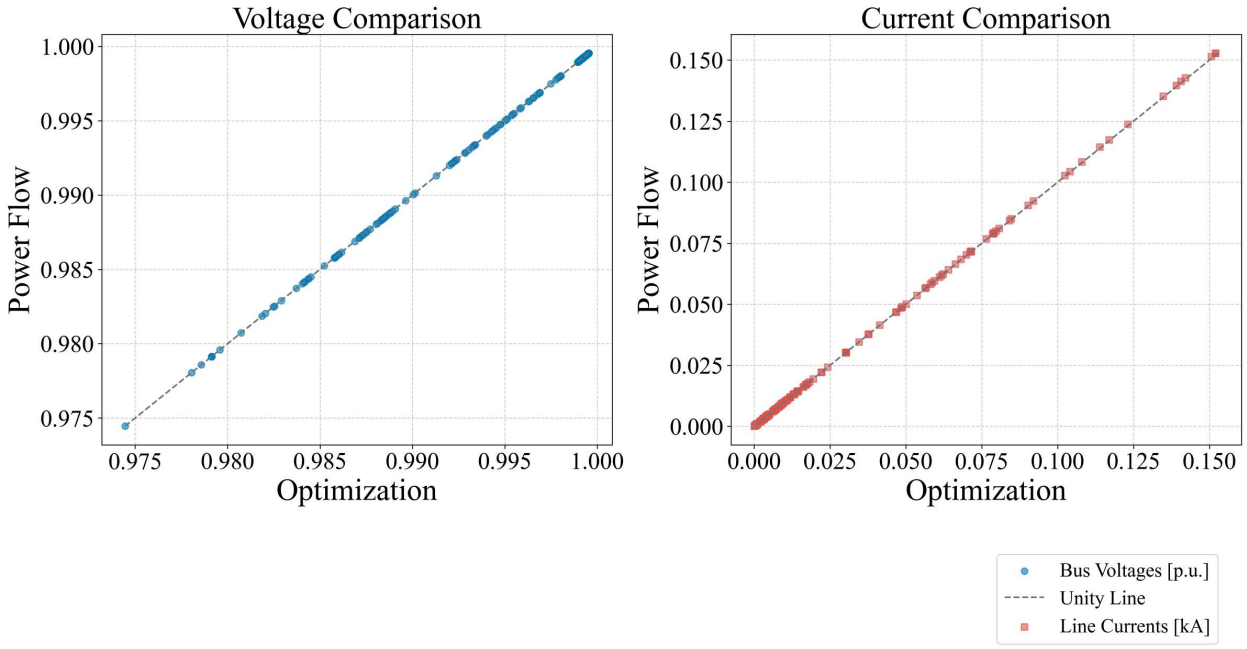

Figure 5.5

5.3 Scalability Analysis

Once the DNEP formulation was linearized, we carried out a scalability analysis to evaluate how the computational burden of the resulting MILP evolves with problem size. The results, presented in Fig. 5.6, illustrate the dependence of problem complexity on two main dimensions: the spatial one, defined by the number of districts, and the temporal one, corresponding to the number of representative days.

The analysis reveals distinct scaling behaviors. The number of continuous variables increases proportionally with both dimensions, whereas the binary variables grow only with the number of districts and remain unaffected by the temporal horizon. As a result, the solver runtime scales linearly with the number of representative days but rises exponentially with the number of districts, reflecting the combinatorial complexity introduced by binary investment decisions.

Extrapolating these trends suggests that solving the problem for data spanning seven days and four districts would require roughly three months of continuous computation, not accounting for the memory constraints that such problem sizes would introduce. This highlights the need for the

reduction strategies introduced in the following sections, which aim to limit both the spatial and temporal dimensions while preserving the essential physical and economic fidelity of the model.

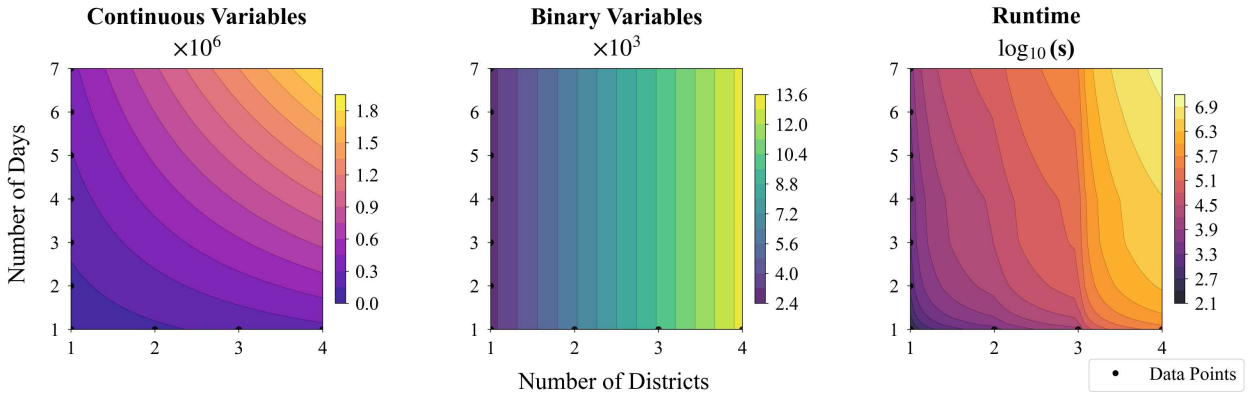

Figure 5.6: Scalability analysis of the linearized DNEP MILP showing how continuous and binary variables, as well as solver runtime, scale with the number of districts and representative days. Continuous variables grow linearly in both dimensions, binary variables only with the number of districts, leading to linear temporal but exponential spatial runtime growth.

5.4 Model Reduction Techniques

5.4.1 Spatial Reduction

To overcome the computational challenge posed by the number of possible line routes, we apply spatial reduction techniques. The goal is to intelligently prune the number of candidate lines to a manageable subset that is still very likely to contain the optimal solution. We implement and compare two methods for this purpose:

Rule-Based Heuristic

The first level of reduction applies a set of intuitive, physically-grounded rules to generate a comprehensive yet manageable set of candidate lines. The rules are as follows:

- Connect every High Voltage (HV) substation to every Medium Voltage (MV) substation.
- Connect MV substations to each other within the same district.
- Connect each MV substation to all MV and LV loads located within the same district.
- Connect each MV load to its two geographically closest MV load neighbors.
- Connect each LV load to its two geographically closest LV load neighbors.

Minimum Spanning Tree (MST) based Reduction

This second, more aggressive method takes the set of lines generated by the rule-based heuristic as its starting point. It iteratively considers each substation as the sole source and finds the shortest possible set of lines (a spanning tree) to connect all loads. The final set of candidate lines is represented by the union of all the resulting trees.

To assess the impact of these reduction methods, we run a targeted experiment. The DNEP model is configured to run on two district, for a single time step, using the base load for each bus. This simplification isolates the effect of the candidate line set on the resulting topology and computational performance.

The results of this experiment, illustrated in Figure 5.7, demonstrate that the reduction of the candidate line set does not deteriorate solution quality. Although the number of candidate lines was progressively reduced—from 160 in the complete configuration to 75 with the rule-based method and 39 with the MST heuristic—the total network cost remained effectively unchanged, with variations below 0.02%. This confirms that the optimal solution lies within the reduced search spaces. The main effect of the reduction is therefore on computational performance: the rule-based method halves the solving time, while the MST heuristic achieves a speed-up of more than one order of magnitude. These results indicate that a carefully designed reduction strategy can substantially improve tractability without compromising optimality

5.4.2 Temporal Reduction: Representative Day Selection

As was proven by the scalability analysis, running the optimization model over a full year is computationally infeasible. On the other hand, we cannot isolate critical timestep because this would mean losing the time domain, rendering modeling the storage dynamic impossible. We must therefore select a small number of representative days. The selection is based on two key annual time-series: the aggregated campus-wide electricity demand and the corresponding solar irradiance profile. We compare two distinct methods for this temporal reduction:

Statistical Distribution Matching

This optimization-based method selects a small, weighted set of days whose combined statistical properties mirror the full annual data. By minimizing the deviation between the cumulative distribution functions (CDFs) of the full year and the selected days, this approach ensures that the frequency and magnitude of various load and generation conditions are accurately preserved. Its strength lies in providing a robust estimation of annual operational costs (OPEX).

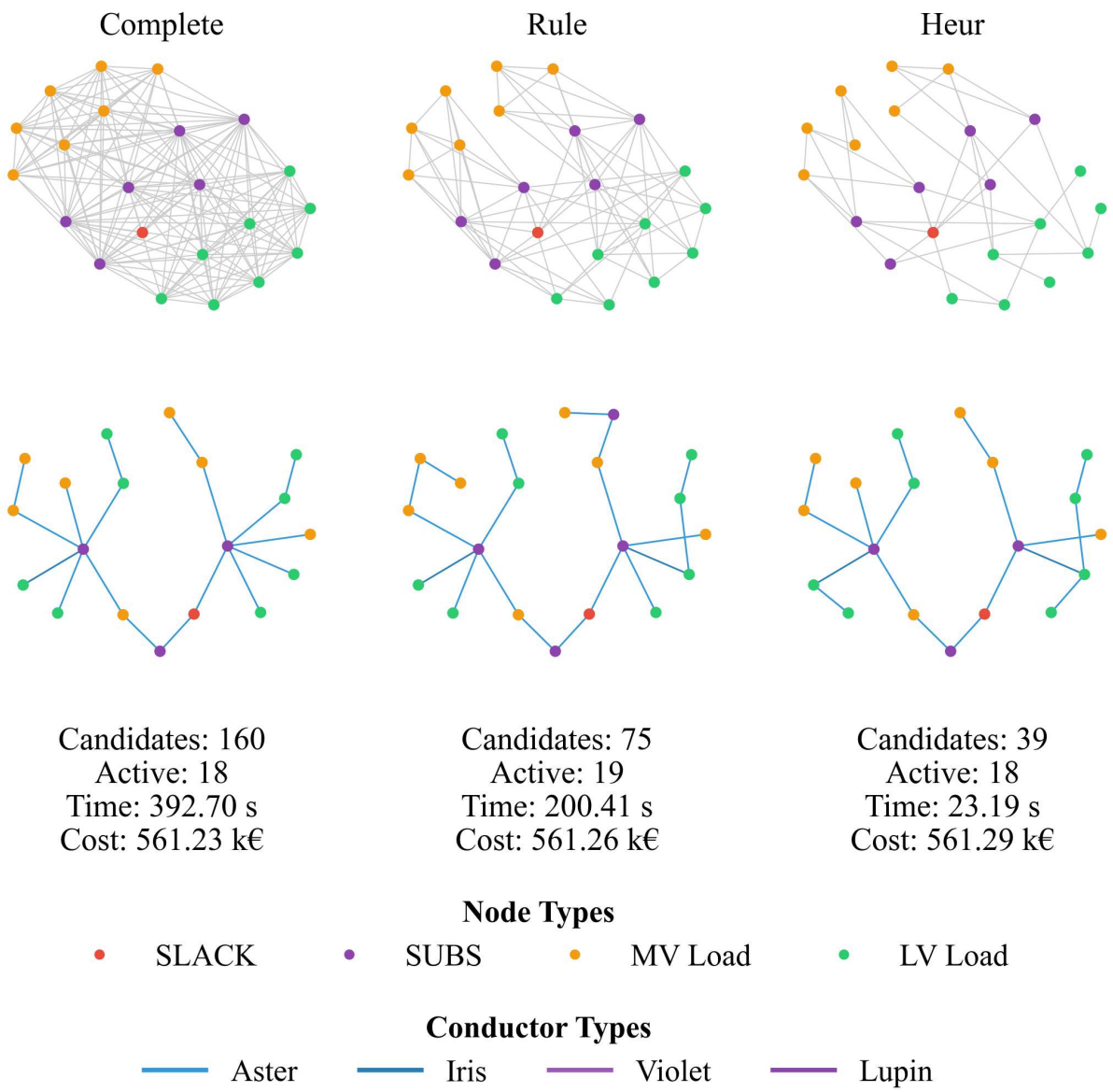

Figure 5.7: Comparison of the spatial reduction methods showing the generated candidate line sets and the resulting optimal topologies. The associated number of candidate and active lines, execution time, and total cost are also reported.

Extreme Day Selection

This clustering-based method prioritizes network robustness over reproducing OPEX. All 365 days are grouped into clusters based on aggregated demand and solar irradiance profiles. From each cluster, the "extreme" day—defined as the day furthest from the clusters center—is selected. By designing the grid to withstand these extreme conditions, the method increases the likelihood that the resulting network will perform reliably under all conditions throughout the year, thus helping to preserve the true grid capital expenditure (CAPEX).

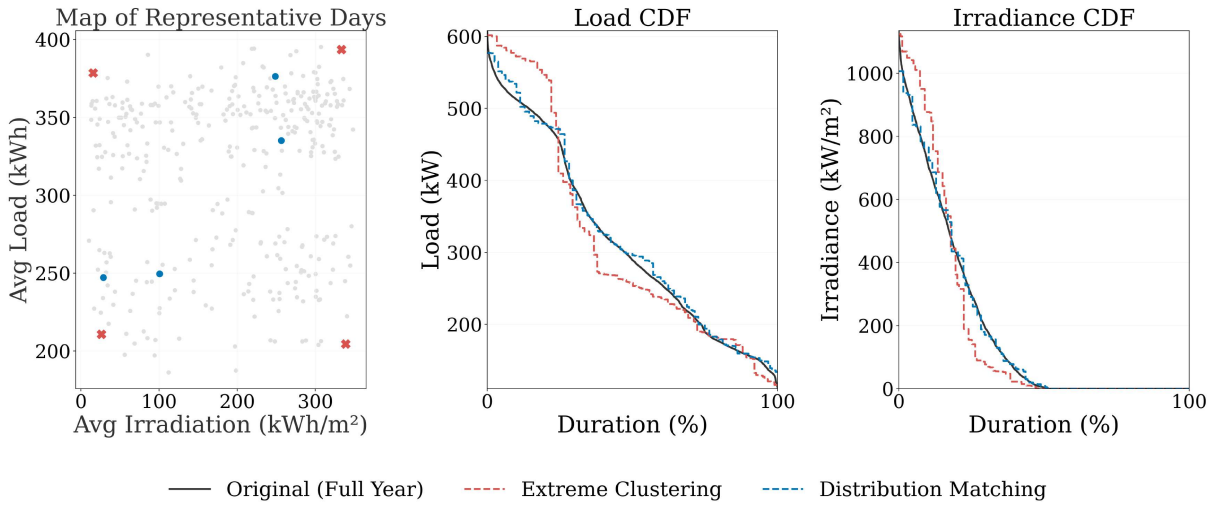

Figure 5.8: Statistical comparison of representative days selection methods

To compare these two methods, the model was run for a single district, using an increasing number of representative days. For this experiment, a simple tariff scheme was used where grid users only pay for their net consumed energy at the wholesale market price. The resulting designs are then evaluated based on their total CAPEX and OPEX for both the DSO and grid users. The plot below highlights the trade-off between designing for cost-efficiency versus resilience.

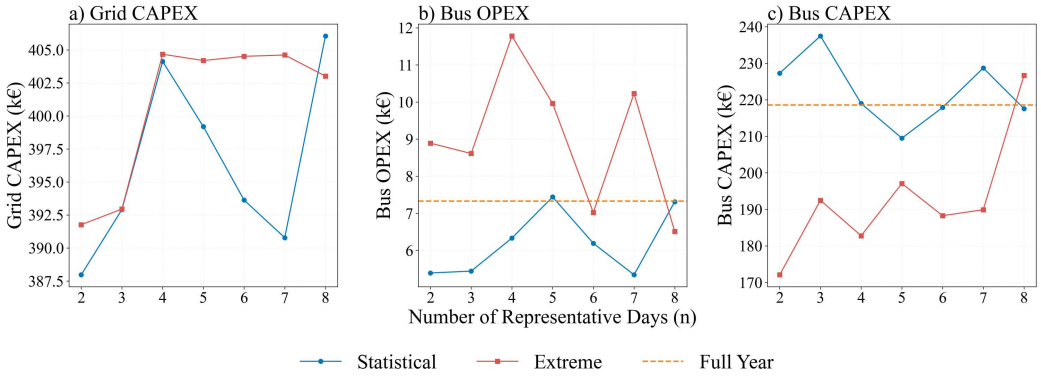

Figure 5.9: Comparison of CAPEX and OPEX for the DSO and Grid User under extreme and statistical day selection methods.

From Figure 5.4 b we can confirm our expectations: the extreme days method is better at identifying stressful condition, thus the grid CAPEX is generally higher and show smaller variance. On the other hand this method has a greater variation in terms of OPEX and the statistical one is on average closer to the full year values.

5.5 Heuristic for Accelerated Convergence

Despite the reductions introduced, the final MILP remains large. To facilitate convergence, a heuristic is developed to provide a high-quality initial solution:

1. **Initial Run:** Solve the model assuming only the best (most expensive) conductor type for all lines.
2. **Fix Topology:** Fix the resulting optimal topology.
3. **Iterative Downgrade:** Iteratively downgrade conductor types on the least-loaded lines, re-solving after each change to verify feasibility and total cost.
4. **Select Best Guess:** Choose the feasible configuration with the lowest total cost and feed it to the full optimization as a warm start.

This procedure reliably accelerates convergence without compromising optimality.

Chapter 6

Results

6.1 Model Parameters and Tariff Definition

Running the optimization framework requires defining two groups of parameters. The first group concerns the techno–economic parameters of all grid and prosumer assets, together with the wholesale price of energy exchanged at the HV substation. These values determine the economic environment in which both the DSO and the prosumers operate. They are reported in Table 6.1.

Parameter	**Value**
Planning horizon (DSO)	30 years
HV substation capacity cost	1000 k€/MVA
MV substation capacity cost	1500 k€/MVA
STATCOM capacity cost	3200 k€/MVAr
HV substation installation cost	50 k€/unit
MV substation installation cost	500 k€/unit
Import/export price at HV substation	0.15 €/kWh
Inverter capacity cost	0.16 k€/kVA
PV capacity cost	0.1 k€/m^2
Storage capacity cost	0.44 k€/kW
PV installation cost	1 k€/unit
Storage installation cost	1.5 k€/unit
Storage efficiency	0.90

Table 6.1: Techno-economic parameters used in the simulations.

The second group of parameters defines the tariff structure used in the decentralized prosumer

optimizations. Tariffs are composed of two terms: an energy-based charge applied to exchanged energy and a capacity-based charge applied to the maximum exchanged power. To allow for different pricing of imported and exported energy, each tariff is defined by the three parameters

$$(\pi_{\text{imp}},\ \pi_{\text{exp}},\ \pi_{\text{cap}}).$$

To systematically study tariff effects, we construct a two–dimensional tariff space. The import rate is fixed at $\pi_{\text{imp}} = 3.0\,\text{c€/kWh}$, while the import–export spread and the capacity fee vary over the discrete sets

$$\Delta\pi = [0.00,\ 0.10,\ 0.20,\ 0.25]\,\text{€/kWh}, \qquad \pi_{\text{cap}} = [0,\ 50,\ 100,\ 200]\,\text{€/kW/year}.$$

The corresponding export rate is $\pi_{\text{exp}} = \pi_{\text{imp}} - \Delta\pi$, and the full set of tariff scenarios is given by the Cartesian product

$$\mathscr{T} = \Delta\pi \times \pi_{\text{cap}}.$$

Each tariff in $\mathscr{T}$ produces a full network design, this is characterized by its topology, the selected conductor types, and the siting and rating of grid assets such as substations and STATCOM units. On the prosumer side, each bus is equipped with an optimized set of LCTs, and their correspondent hourly dispatch vectors.

While each bus and consequently each feeder exhibits its own operational behaviour, analysing such detailed dynamics is not the first scope of this thesis. Our primary objective is to assess how different economic signals shape the overall cost structure of the system. We therefore begin the analysis from the aggregated cost components, which compactly summarize how investments and operations respond to the tariff signal.

6.2 Aggregated Cost Gaps

Figure 6.1 summarizes the results of the tariff sweep. Each heatmap reports the gap between the decentralized and the centralized solution for the main cost components. The TSC map provides an immediate indication of which tariff structures yield the most efficient decentralized outcome. The lowest total system cost is obtained for tariffs with high spread and no capacity fee, as seen in the bottom–right corner of the TSC heatmap. To understand why this specific combination performs best, we proceed by analyzing the disaggregated cost gaps.

The OPEX map shows a clear trend: increasing the spread and reducing the capacity fee both lead to lower operational expenses. To interpret this behaviour, we recall that operational costs are

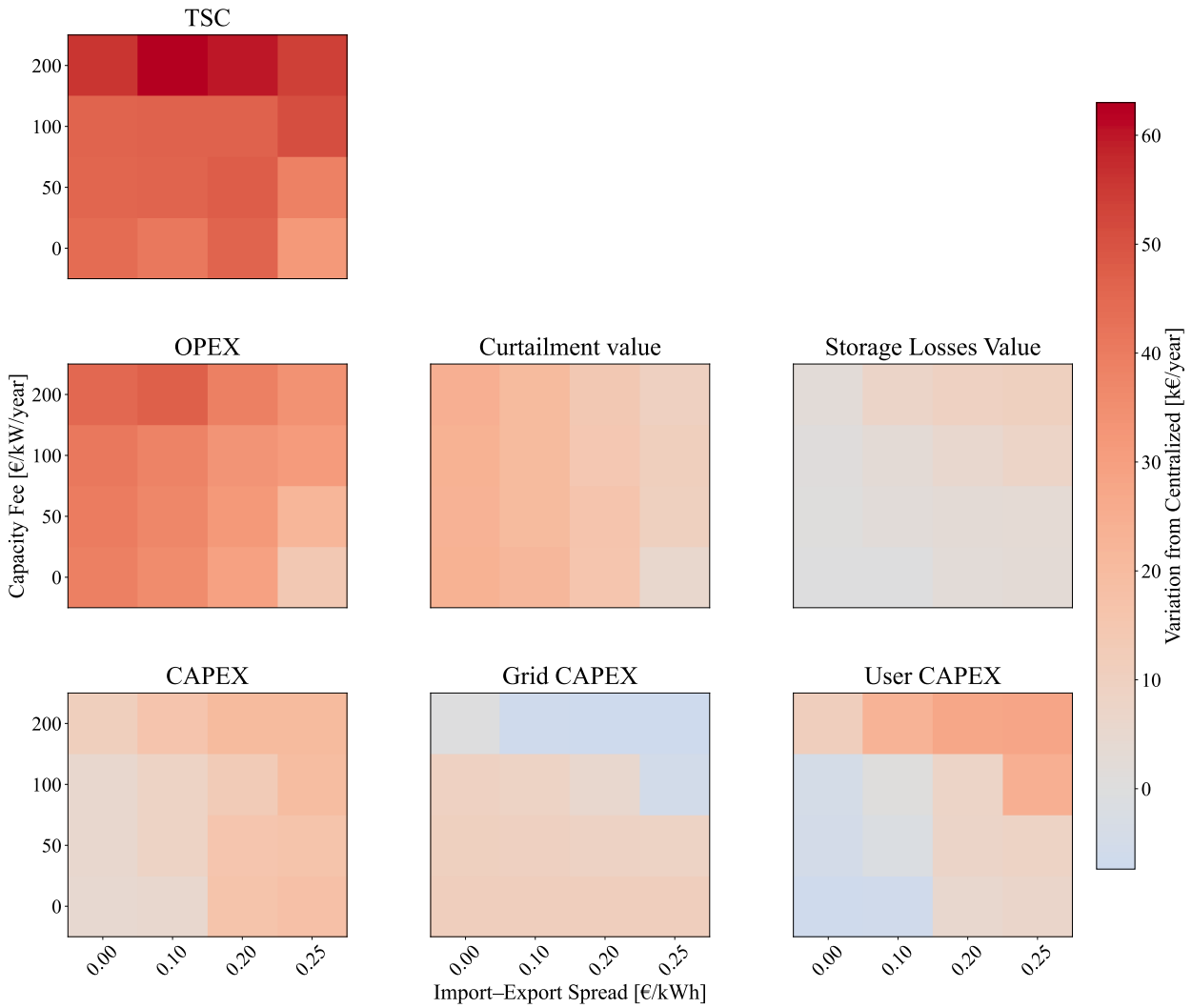

Figure 6.1: Gap between decentralized and centralized solutions for total cost and its components.

driven by imported energy:

$$E_{\text{imp}} = E_{\text{load}} - E_{\text{PV}} + E_{\text{loss,line}} + E_{\text{loss,stor}}.$$

Since loads are identical across all tariffs and line losses are found to be negligible, the variation in OPEX must originate from PV production and storage losses. The curtailment and storage-loss maps in Figure 6.1 confirm this: the dominant factor is PV curtailment, which reduces noticeably with the spread. High curtailment forces the system to import more energy, increasing OPEX. This provides a first important insight: not exploiting available PV potential is the main inefficiency driving operational costs.

Turning to investments, the CAPEX map reveals a different pattern: both a higher spread and a higher capacity fee tend to increase the investment gap. This results from the balance between two

opposite contributions. On the one hand, the grid CAPEX gap decreases with both tariff signals and can even become negative, indicating that decentralized self-consumption and flexibility may reduce the need for grid reinforcement. On the other hand, user CAPEX rises sharply, more than offsetting any potential grid savings. This shows that relying on user-side LCT investments to relieve the grid is not cost-effective at system level: the private asset cost exceeds the avoided grid cost.

Combining these observations leads to a coherent picture. Both economic signals encourage additional LCT deployment, but the associated investment does not reduce total CAPEX, as the savings on the grid are outweighed by user expenditures. The key differentiator between tariffs is therefore operational efficiency. A higher spread increases PV utilisation, reduces imports, and thus lowers OPEX. This explains why tariffs with a high spread and zero capacity fee ultimately yield the most cost-effective decentralized outcome.

6.3 Feeder-Level Analysis

The aggregated results presented so far describe the behaviour of the system when a single tariff is applied uniformly to all users. While this is appropriate for assessing tariff performance at system scale, it is important to note that in our campus dataset several buses exhibit very large PV potentials combined with extremely low loads. Under many tariff configurations, these buses find it economically convenient to not take advantage of their full renewable potential. As a consequence, the system-wide OPEX variation observed in the previous section was strongly influenced by this behaviour.

To obtain a clearer picture of how tariff signals affect other prosumers, we isolate a representative LV feeder where such extreme PV–load ratios do not occur. This feeder is more consistent with a residential setting, where prosumers have moderate PV availability and load profiles that make self-consumption and storage operation comparable to realistic urban or suburban conditions.

Table 6.2 reports the four tariff configurations analysed in this section.

Name	$\Delta\pi$ [€/kWh]	π_{cap} [€/kW/year]
Net Metering (NM)	0.00	0
Net Billing (NB)	0.25	0
NM + Capacity Fee (NM+C)	0.00	200
NB + Capacity Fee (NB+C)	0.25	200

Table 6.2: Tariff combinations analysed at feeder level.

Figure 6.2 shows the cost decomposition associated with these four tariffs for the selected feeder.

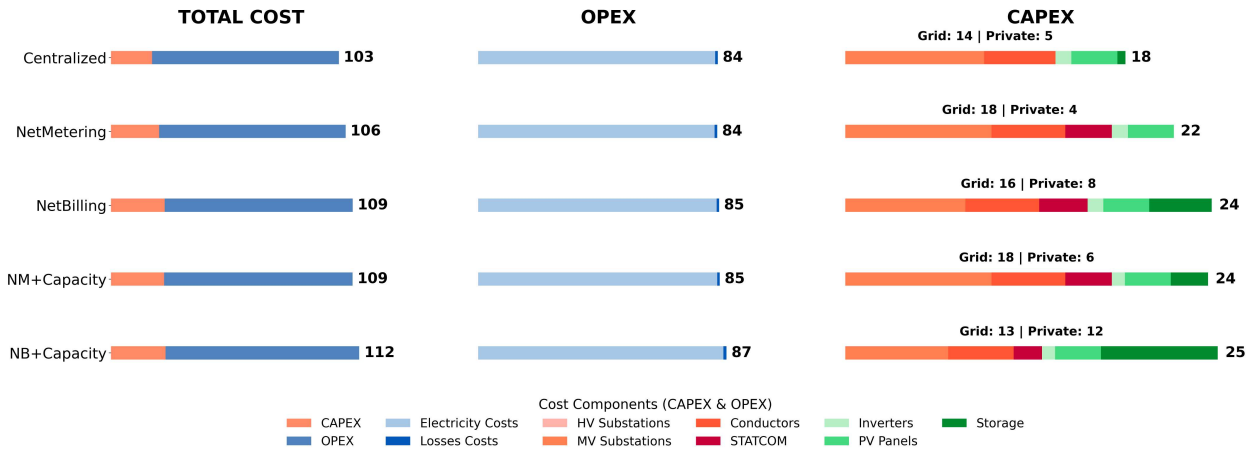

Figure 6.2: Cost decomposition for the four extreme tariffs on the selected LV feeder.

A first observation confirms this expectation. Once we focus on the selected feeder, where PV potential and load are more balanced, prosumers no longer have an incentive to curtail PV under any tariff. Consequently, the OPEX differences across tariffs are not driven by curtailment. In this context, OPEX no longer decreases with higher spreads: the trend is flattened or even reversed as storage losses increase with both the import-export spread and the capacity fee.

Consequently, the Total System Cost on this feeder is primarily determined by the CAPEX variation. Here the same investment trade-off observed earlier reappears: the NM tariffs has the lower gap, as reinforcing the grid is proven to be more cost efficient than installing storage.

Figure 6.3 provides additional insight by reporting the aggregated power flows for the selected feeder under the four tariffs.

These plots highlight two important qualitative differences. First, the reactive power balance shows a clear separation between the centralized and decentralized cases. In the centralized solution, the inverter capacities of distributed LCTs are used to supply or absorb reactive power, keeping net reactive injections near zero. Under all decentralized tariffs, instead, this coordinated use of reactive flexibility does not emerge, leading to the installation and active operation of STATCOM units on the feeder. This confirms that the considered tariffs are not able of coordinating inverter capabilities effectively.

Second, while the centralized case uses storage only to avoid oversizing the grid to by reducing power peaks. Tariff with high spread and capcity fees, induce much more intensive storage cycling driving up losses. In particular, storage operation under NB does not flatten the peak power demanded at the substation, which results in a grid CAPEX similar to the NM case.

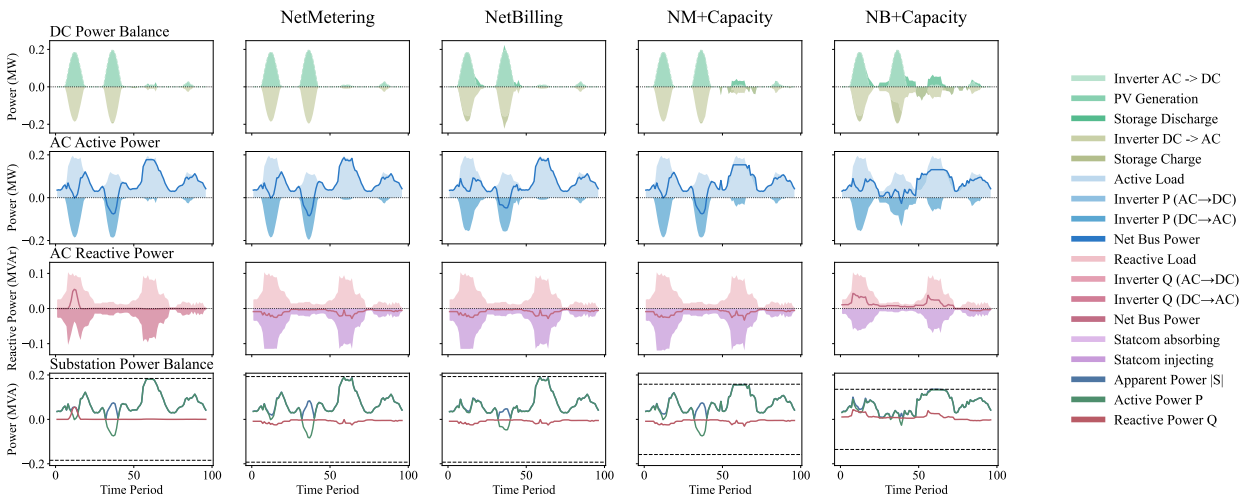

Figure 6.3: Aggregated DC, AC, and substation power flows under the four extreme tariffs.

Overall, this feeder-level analysis reinforces the conclusions drawn earlier: the economic signals under consideration strongly influence prosumer investment and operation, but they do not inherently coordinate these actions in a grid-efficient manner. Even though decentralized LCTs have the technical capability to support the network, the tariff structures tested here do not consistently elicit such behaviour.

Chapter 7

Conclusions

This thesis presented a comparative optimization framework designed to assess how different tariff structures influence prosumer investment behaviour and the resulting evolution of the distribution network. The main contribution of this work lies in the development and validation of a modelling tool capable of quantifying the degree of alignment between decentralized decisions and the system-wide optimum. The numerical results discussed throughout the thesis are therefore intended as illustrative outcomes of the methodology rather than as definitive predictions for any real system, as their validity is inherently tied to the techno-economic assumptions and to the characteristics of the dataset employed.

By contrasting decentralized and centralized regimes, the framework computes a transparent measure of the coordination gap induced by alternative tariff schemes. The case study confirms that different economic signals lead prosumers to adopt markedly different operational and investment strategies—affecting PV utilisation, self-consumption, storage cycling, and peak grid usage—and that these behavioural shifts translate into heterogeneous reinforcement requirements for the distribution network. In particular, the analysis shows that not exploiting available PV potential is the dominant source of inefficiency in decentralized operation, that a spread between import and export tariffs does not effectively reduce feeder peak loads, and that the considered tariff structures fail to coordinate the reactive capabilities of inverters, leaving substantial potential for grid-supportive behaviour untapped.

At the same time, the modelling exercise highlighted a number of structural simplifications that limit the realism of the current formulation. These limitations also identify clear directions for future extensions of the framework.

7.1 Model Limitations and Directions for Development

Representation of technical constraints. Several technical components were simplified to ensure computational tractability. For instance, inverter operation was modelled using reduced sets of constraints that do not capture the full complexity of device capabilities, control strategies, or grid-code requirements. Incorporating more realistic inverter behaviour would allow for a more precise assessment of the flexibility that distributed assets can provide.

Energy prices and market-driven dynamics. The model assumes constant import and export prices over the entire planning horizon. However, wholesale energy prices are time-varying and respond to market dynamics and renewable variability. Using fixed prices prevents the framework from capturing interactions between tariff design, arbitrage potential, and market conditions. Extending the model to incorporate time-varying prices or simplified market coupling would enable a more complete evaluation of tariff performance.

From greenfield to brownfield planning. The case study adopted a greenfield planning perspective to isolate the impact of tariffs from legacy infrastructure. Real-world DSOs operate in brownfield environments, where existing networks constrain reinforcement decisions. Extending the framework to accommodate brownfield conditions—such as fixed line routes, existing asset capacities, and multi-stage investment decisions—would significantly expand its practical relevance.

Bibliography

[1] IPCC, 2023: Climate Change 2023: Synthesis Report. Contribution of Working Groups I, II and III to the Sixth Assessment Report of the Intergovernmental Panel on Climate Change [Core Writing Team, H. Lee and J. Romero (eds.)]. IPCC, Geneva, Switzerland, pp. 35-115, doi: 10.59327/IPCC/AR6-9789291691647.

[2] European Commission. (2025, June). Climate change (Special Eurobarometer 565). https://europa.eu/eurobarometer/surveys/detail/3472

[3] International Energy Agency, *World Energy Outlook 2024*. IEA, 2024.

[4] Thoning, K. W., Crotwell, A. M., and Mund, J. W., 2025: *Atmospheric Carbon Dioxide Dry Air Mole Fractions from continuous measurements at Mauna Loa, Hawaii*. NOAA Global Monitoring Laboratory. Version 2025-04-26, doi:10.15138/yaf1-bk21.

[5] Lan, X., Thoning, K. and Dlugokencky, E. J., 2025: *Trends in globally-averaged CH4, N2O, and SF6 determined from NOAA Global Monitoring Laboratory measurements*. Version 2025-07, NOAA Global Monitoring Laboratory, doi:10.15138/P8XG-AA10.

[6] The European Parliament and the Council of the European Union, 2021: *Regulation (EU) 2021/1119 of the European Parliament and of the Council of 30 June 2021 establishing the framework for achieving climate neutrality and amending Regulations (EC) No 401/2009 and (EU) 2018/1999 ('European Climate Law')*. Official Journal of the European Union, L 243, pp. 1-17.

[7] The European Parliament and the Council of the European Union, 2023: *Directive (EU) 2023/2413 of 18 October 2023 amending Directive (EU) 2018/2001, Regulation (EU) 2018/1999 and Directive 98/70/EC as regards the promotion of energy from renewable sources, and repealing Council Directive (EU) 2015/652 (RED III)*. Official Journal of the European Union, L 2023/2413, pp. 1–146.

[8] European Commission, 2018: *In-depth analysis in support of the Commission Communication COM(2018) 773: A Clean Planet for all - A European long-term strategic vision for a prosperous, modern, competitive and climate neutral economy*. European Commission, Brussels.

[9] European Court of Auditors, 2023: *The EU's support for sustainable biofuels in transport - An unclear path ahead*. Special Report 29/2023, Publications Office of the European Union, Luxembourg.

[10] European Court of Auditors, 2024: *The EU's industrial policy on renewable hydrogen*. Special Report 11/2024, Publications Office of the European Union, Luxembourg.

[11] Butorac, S., 2025: *EU electricity grids*. Briefing PE 772.854, European Parliamentary Research Service, European Parliament, Brussels.

[12] E-distribuzione S.p.A., 2024: *Piano di Sviluppo 2025 della rete di distribuzione*. Roma, Italia.

[13] T. D. de Lima, F. Lezama, J. Soares, J. F. Franco, and Z. Vale, "Modern distribution system expansion planning considering new market designs: Review and future directions," *Renewable and Sustainable Energy Reviews*, vol. 202, p. 114709, 2024.

[14] J. M. Nahman and D. M. Peric, "Optimal Planning of Radial Distribution Networks by Simulated Annealing Technique," *IEEE Transactions on Power Systems*, vol. 23, no. 2, pp. 790-795, May 2008.

[15] A. Soroudi, A. Keane and M. Power, "Multi-Stage Rolling Grid Expansion Planning for Distribution Networks Considering Conditional Value at Risk," *IEEE Transactions on Power Systems*, vol. 27, no. 3, pp. 1583-1592, Aug. 2012.

[16] J. F. Franco, M. J. Rider, and R. Romero, "A mixed-integer quadratically-constrained programming model for the distribution system expansion planning," *Electrical Power and Energy Systems*, vol. 62, pp. 265-272, 2014.

[17] G. Muñoz-Delgado, J. Contreras, and J. M. Arroyo, "Joint Expansion Planning of Distributed Generation and Distribution Networks," *IEEE Transactions on Power Systems*, vol. 30, no. 5, pp. 2579-2590, Sept. 2015.

[18] M. A. Mejía, L. H. Macedo, G. Munoz-Delgado, J. Contreras and A. Padilha-Feltrin, "Multistage Planning Model for Active Distribution Systems and Electric Vehicle Charging Stations Considering Voltage-Dependent Load Behavior," *IEEE Transactions on Smart Grid*, vol. 13, no. 2, pp. 1383-1397, March 2022.

[19] H. Yao, Y. Xiang, C. Gu and J. Liu, "Optimal Planning of Distribution Systems and Charging Stations Considering PV-Grid-EV Transactions," *IEEE Transactions on Smart Grid*, vol. 16, no. 1, pp. 691-704, Jan. 2025.

[20] Y. Lavi and J. Apt, "Using PV inverters for voltage support at night can lower grid costs," *Energy Reports*, vol. 8, pp. 6347-6354, 2022.

[21] A. Arefi, A. Abeygunawardana and G. Ledwich, "A New Risk-Managed Planning of Electric Distribution Network Incorporating Customer Engagement and Temporary Solutions," in IEEE Transactions on Sustainable Energy, vol. 7, no. 4, pp. 1646-1661, Oct. 2016.

[22] H. Haghighat and B. Zeng, "Stochastic and Chance-Constrained Conic Distribution System Expansion Planning Using Bilinear Benders Decomposition," *IEEE Transactions on Power Systems*, vol. 33, no. 3, pp. 2696-2705, May 2018.

[23] I. J. Ramírez-Rosado and J. L. Bernal-Agustin, "Genetic algorithms applied to the design of large power distribution systems," *IEEE Transactions on Power Systems*, vol. 13, no. 2, pp. 696-703, May 1998.

[24] M. E. Samper and A. Vargas, "Investment Decisions in Distribution Networks Under Uncertainty With Distributed Generation—Part II: Implementation and Results," *IEEE Transactions on Power Systems*, vol. 28, no. 3, pp. 2341-2351, Aug. 2013.

[25] M. Lavorato, M. J. Rider, A. V. Garcia and R. Romero, "A Constructive Heuristic Algorithm for Distribution System Planning," *IEEE Transactions on Power Systems*, vol. 25, no. 3, pp. 1734-1742, Aug. 2010.

[26] The European Parliament and the Council of the European Union, "Directive (EU) 2019/944 of the European Parliament and of the Council of 5 June 2019 on common rules for the internal market for electricity and amending Directive 2012/27/EU," *Official Journal of the European Union*, L 158/125, 2019.

[27] ACER, "Report on Distribution Tariff Methodologies in Europe," European Union Agency for the Cooperation of Energy Regulators, Ljubljana, Slovenia, Feb. 2021.

[28] B. Zeng, J. Shi, J. Wen and J. Zhang, "A game-theoretic framework for active distribution network planning to benefit different participants under the electricity market," *Turkish Journal of Electrical Engineering and Computer Sciences*, vol. 25, pp. 83-94, 2017.

[29] M. Cornet, G. Bailly, M. Glavic, B. Cornélusse, "A one-leader multi-follower approach to distribution network development planning," in *2023 IEEE PES Innovative Smart Grid Technologies Europe (ISGT EUROPE)*, Grenoble, France, 2023, pp. 1-5.

[30] S. Mathieu, Q. Louveaux, D. Ernst, and B. Cornélusse, ”DSIMA: A testbed for the quantitative analysis of interaction models within distribution networks,” *Sustainable Energy, Grids and Networks*, vol. 5, pp. 78–93, 2016

[31] R. J. Hennig, S. H. Tindemans, and L. J. de Vries, “Market Failures in Local Flexibility Market Proposals for Distribution Network Congestion Management,” in *Proceedings of the 18th International Conference on the European Energy Market (EEM)*, Sept. 2022, doi: 10.1109/EEM54602.2022.9920980.